Геомодель

Санкт-Петербург 2024

Геонауки: современные вызовы и пути решений

11-я международная конференция

8-11 апреля 2024 года | Санкт-Петербург, Россия

www.geomodel.ru

Геомодель

2024 Санкт-Петербург

Noise resistance and microcracks localization accuracy while hydrofracturing of layers using intellectual robot “ADEE”

A.A.Tabakov, Yu.A. Stepchenkov, V.N. Ferentzy

ГеоВерс

St. Petersburg, 2024

Introduction

Microseismic monitoring becomes last years more and more important for Controlling of Hydfractored Cracks (CHC), mines safety control, monitoring of gas storages, and so on.

CHC in Russia is not supplied with adequate software for accurate, noise resistant and reliable localization of cracking events, as well as for designing of optimal field acquisition geometry and objective estimate of localization results.

Here presented are results of application the Intellectual Robot (IR) ADEE (Analysis, Decision, Execution, Estimation) for real time automatic localization of modeled cracking events.

Configuration of probability space fields for linear (borehole) and areal (surface) arrays were calculated. Accuracy of cracks localization was estimated for different signal to white noise ratio. Acceptable level of localization errors for 21-sensor linear array was 0.2 and for 204-sensor surface array was 0.04.

Presented software was developed on UNIVERS platform.

1. Borehole array Method

Borehole observations provide sufficient advantages compared to surface ones due to lower noise level.

But borehole array is a linear antenna with poor only polar selectivity in lateral directions.

Accuracy and noise resistance of fully automatic Intellectual Robot ADEE were tested on model data. Geometry of simulated array is on Fig.1.

Wave fields generated by several sources walking away from depth 1200 m in vertical fractured well were calculated for vertical array 200 m away from sources. The sources are spread out on horizontal circle centered on observation well. Magnitude of short right sided 60 Hz signals decreased approximately two times on each next 8 positions (Table 1) .

Fig. 2 depicts wavefields for 21-receiver array on a base 400 m in tracking component.

Receiver array is symmetrical relatively to center on depth 1000 m. Accuracy of events localization was estimated for different number of receivers on different bases versus signal to white noise ratio.

Geometry of borehole observations

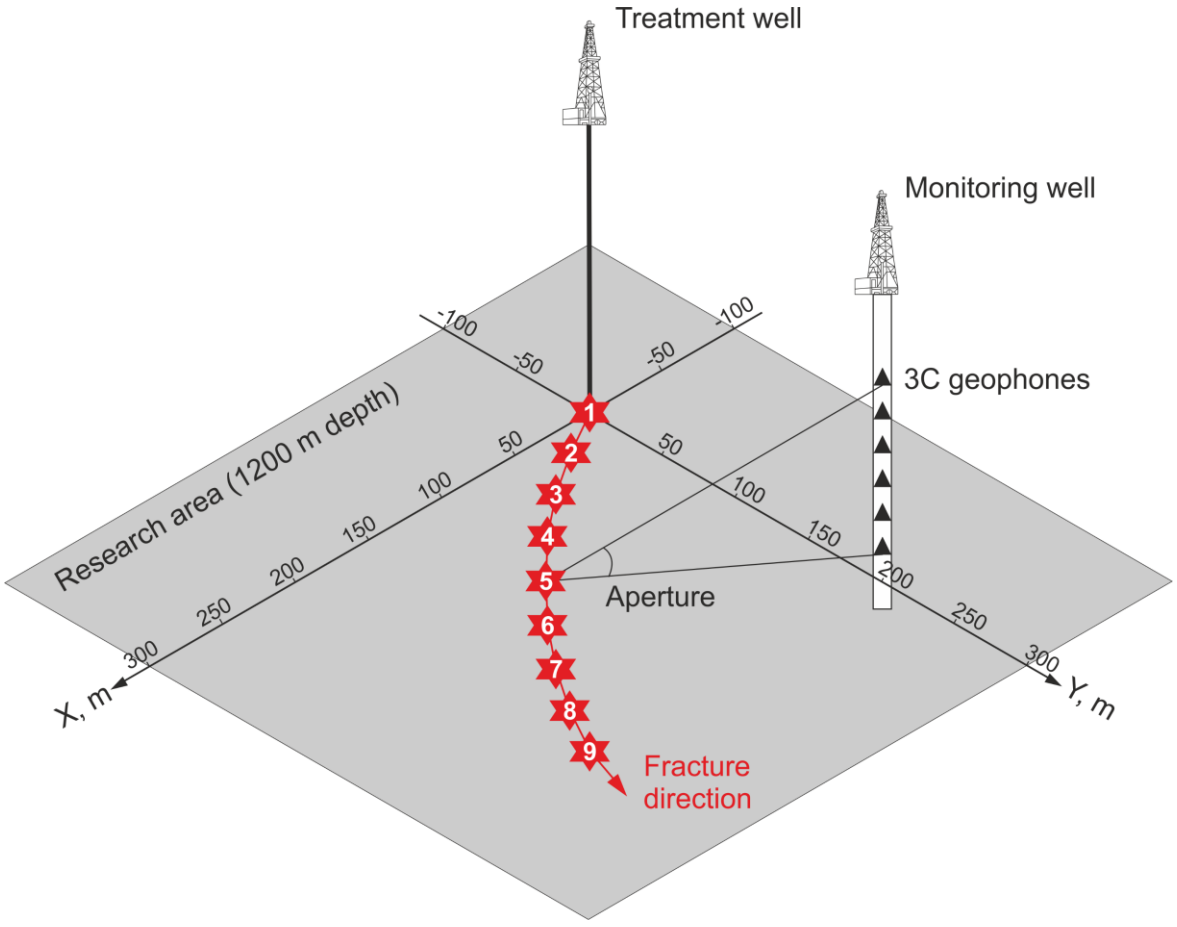

Fig.1. Geometry of borehole observations

Model wavefield

Pressure waves

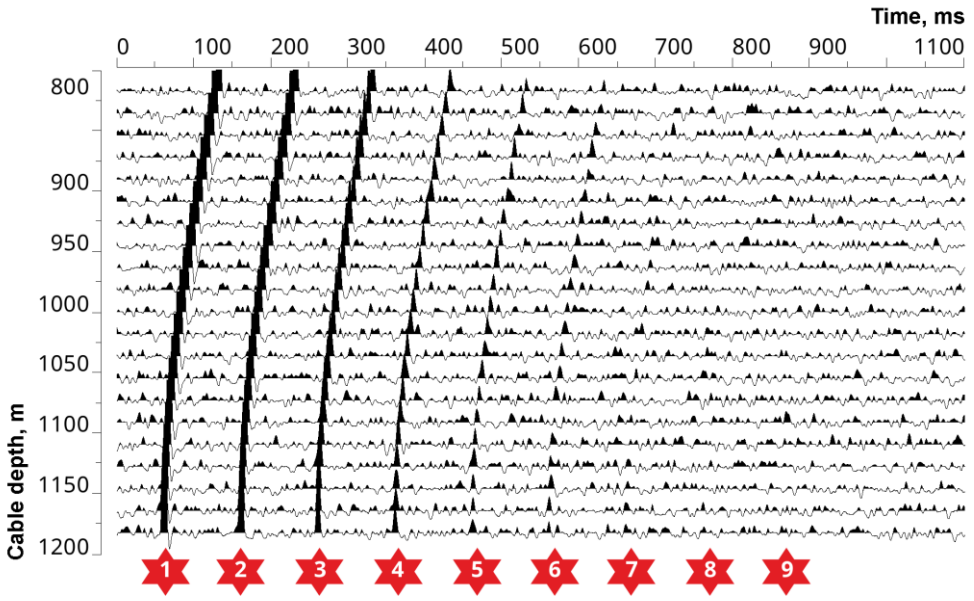

Shear waves

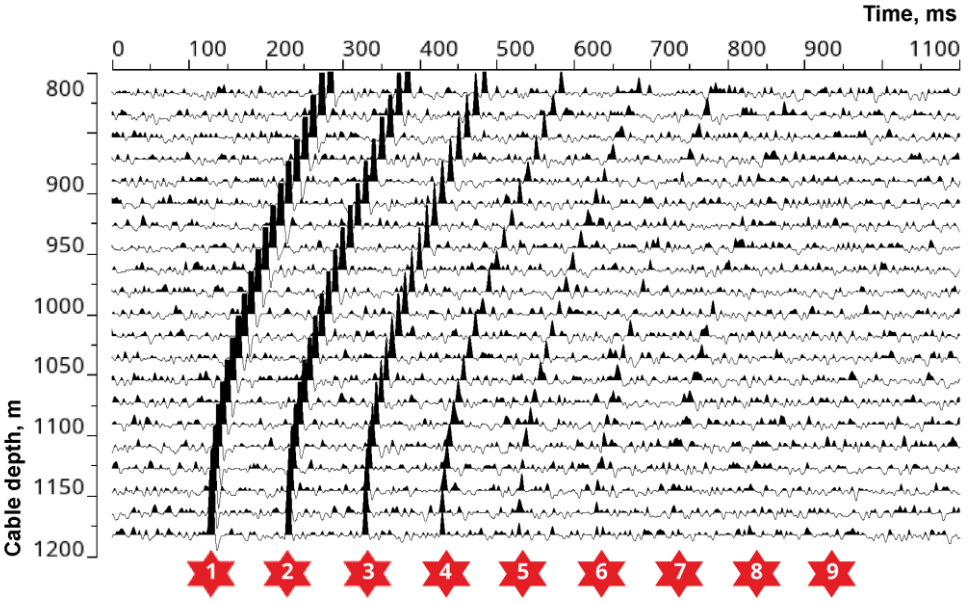

Fig. 2.Model wavefields (follow up component)

Table 1.Signal to noise ratios

Event №	1	2	3	4	5	6	7	8	9
s / n	10	5	2.5	1.25	0.8	0.6	0.4	0.2	0.1

Probability fields for first event

Intellectual Robot ADEE produced in three orthogonal planes (Fig.3) for the first source, registered by 21-levels array on the base 400 m.

Probability fields show:

- Lateral uncertainty higher then in a vertical plane.
- Uncertainty for shear waves less then for pressure waves.
- Uncertainty for shear and pressure waves together less then otherwise.

Fields of probability

Pressure waves

Shear waves

Both pressure and shear waves

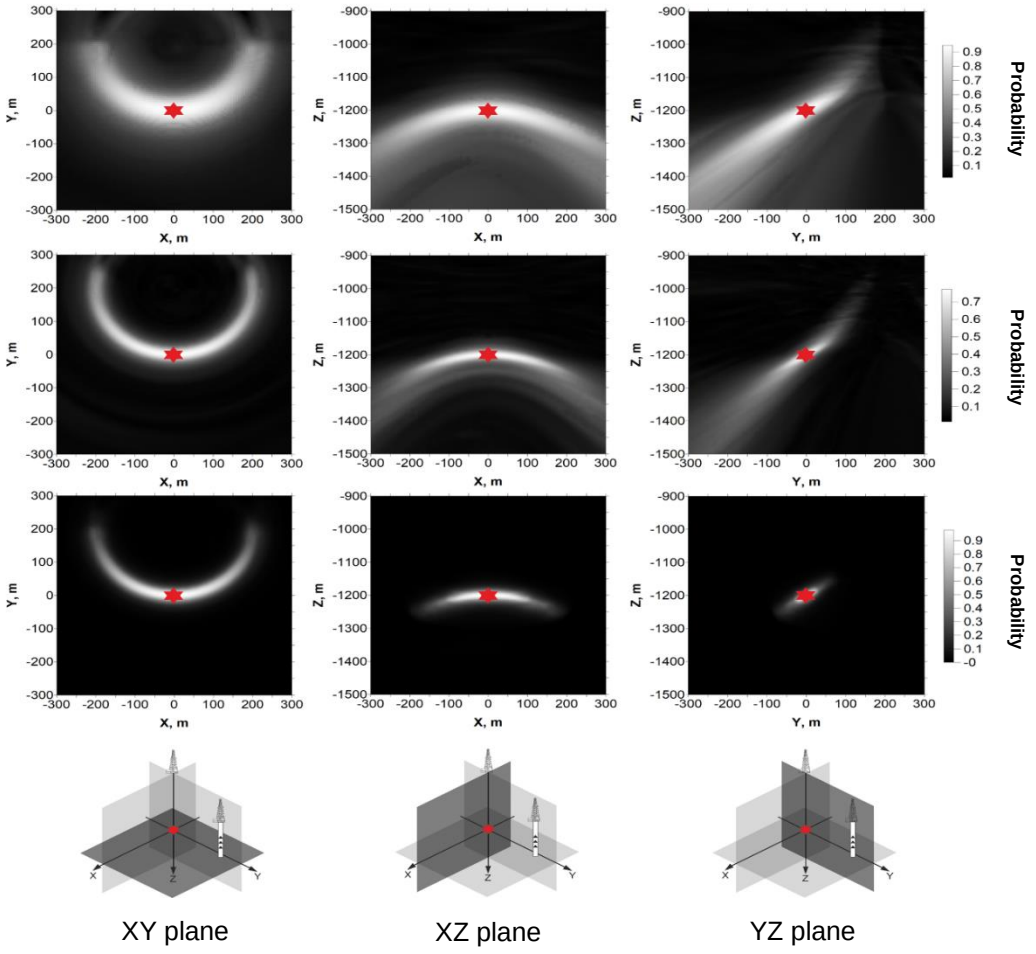

Fig. 3. Probability fields for the first event (21-sensors geophone, 400 m spatial base, 60^0 aperture)

Localized microseismic events

Determined by ADEE positions of all 9 sources with decreasing s/n ratio presented on Fig. 4.

- Actually accurate localization may be achieved for s/n=0.2, though events cannot entirely be found in registered wavefield;
- Almost exact localization of offsets take place but laterally there are small variations.

Localized microseismic events

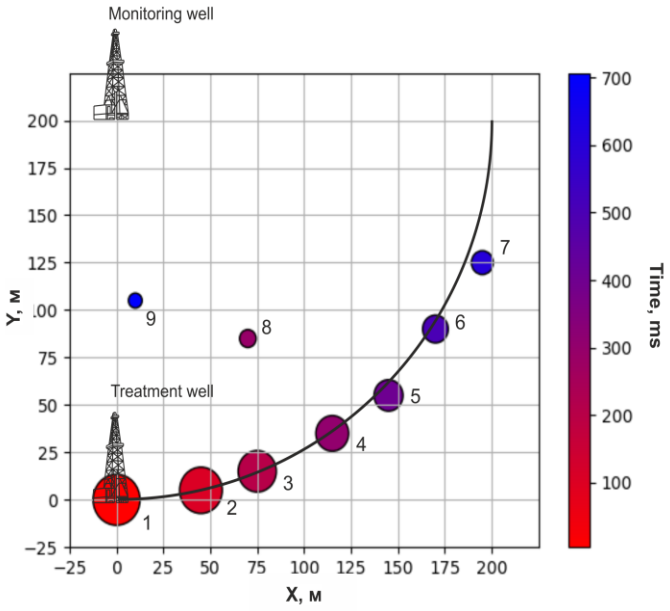

Pressure waves

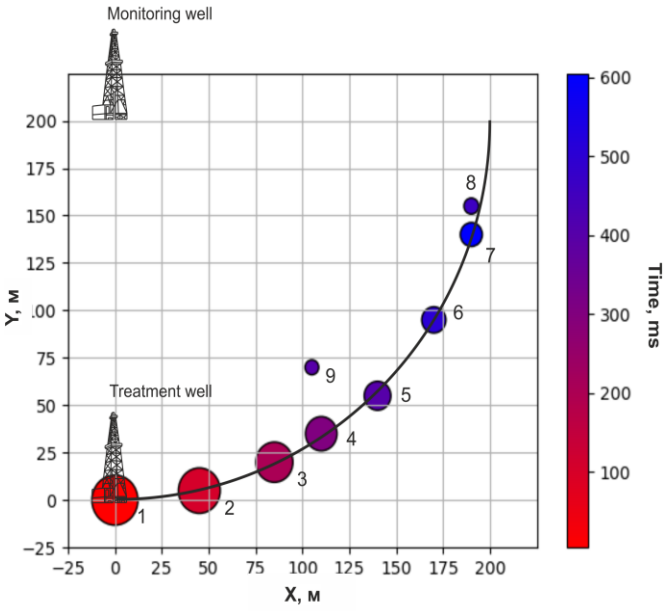

Shear waves

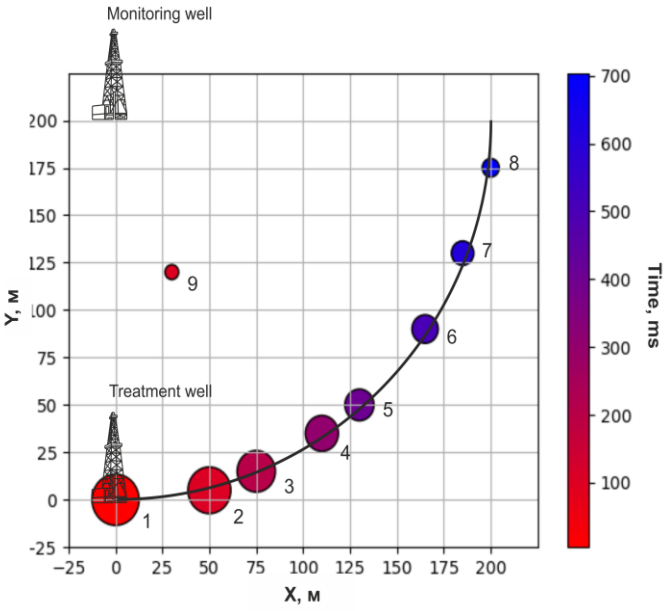

Both pressure and shear waves

Event №	1	2	3	4	5	6	7	8	9
s / n	10	5	2.5	1.25	0.8	0.6	0.4	0.2	0.1

Fig. 4. Expected localization points for the events (21-sensors geophone, 400 m spatial base)

Signal selection from the events

After localization of events, it becomes possible to calculate the trajectories of each event in the wave field and estimate the waveform for it, generally three-component.

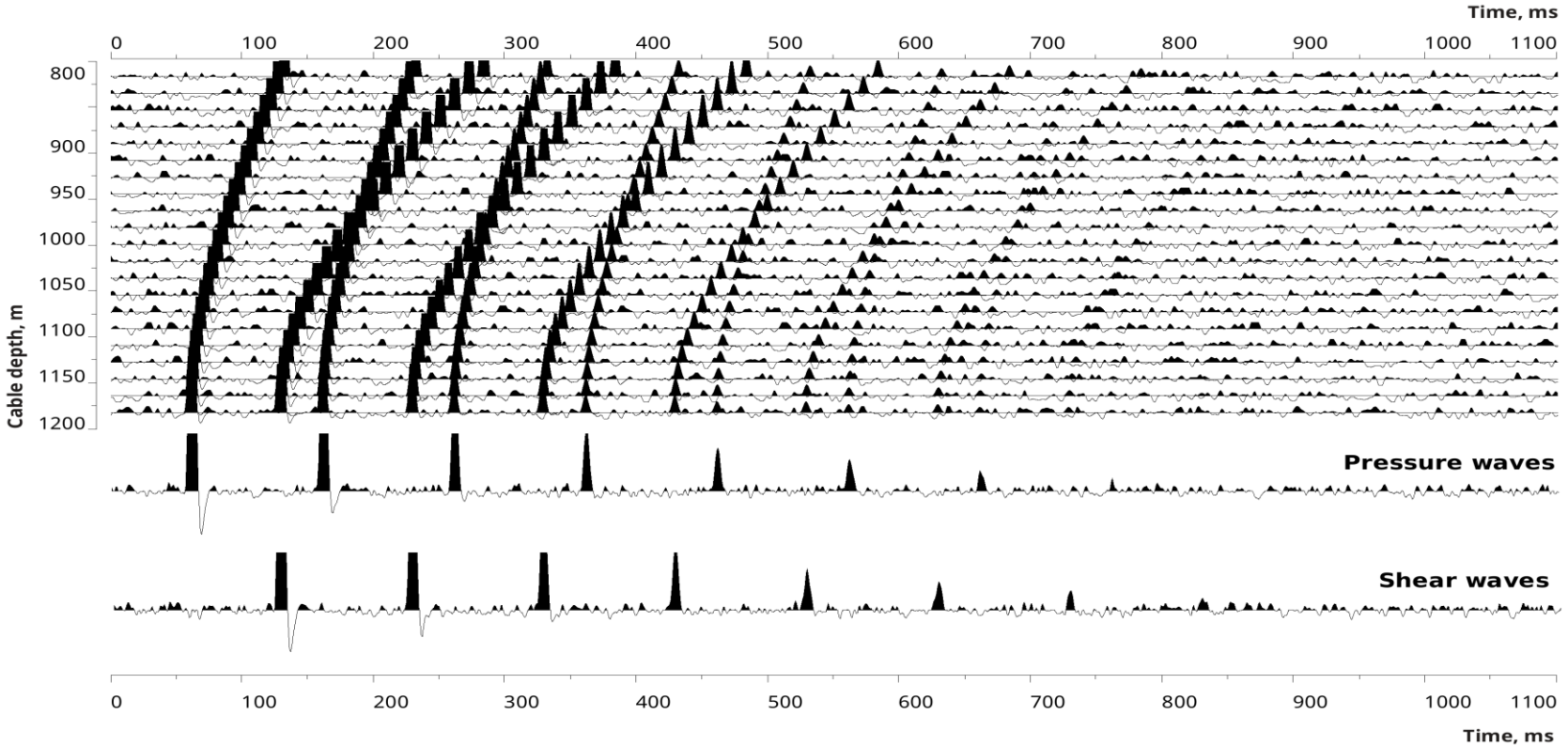

Fig. 5. Microseismic events waveforms

Deviations of estimated and predetermined locations of microseismic events

Depicted on Figure 6 are averaged from 10 different realizations of white noise deviations of locations, determined by IR ADEE from predetermined for pressure, shear waves and combined.

Deviations more then 25 m marked as not reliable.

Deviations of the estimated centers of microseismic events from the specified

Pressure waves

Shear waves

Both pressure and shear waves

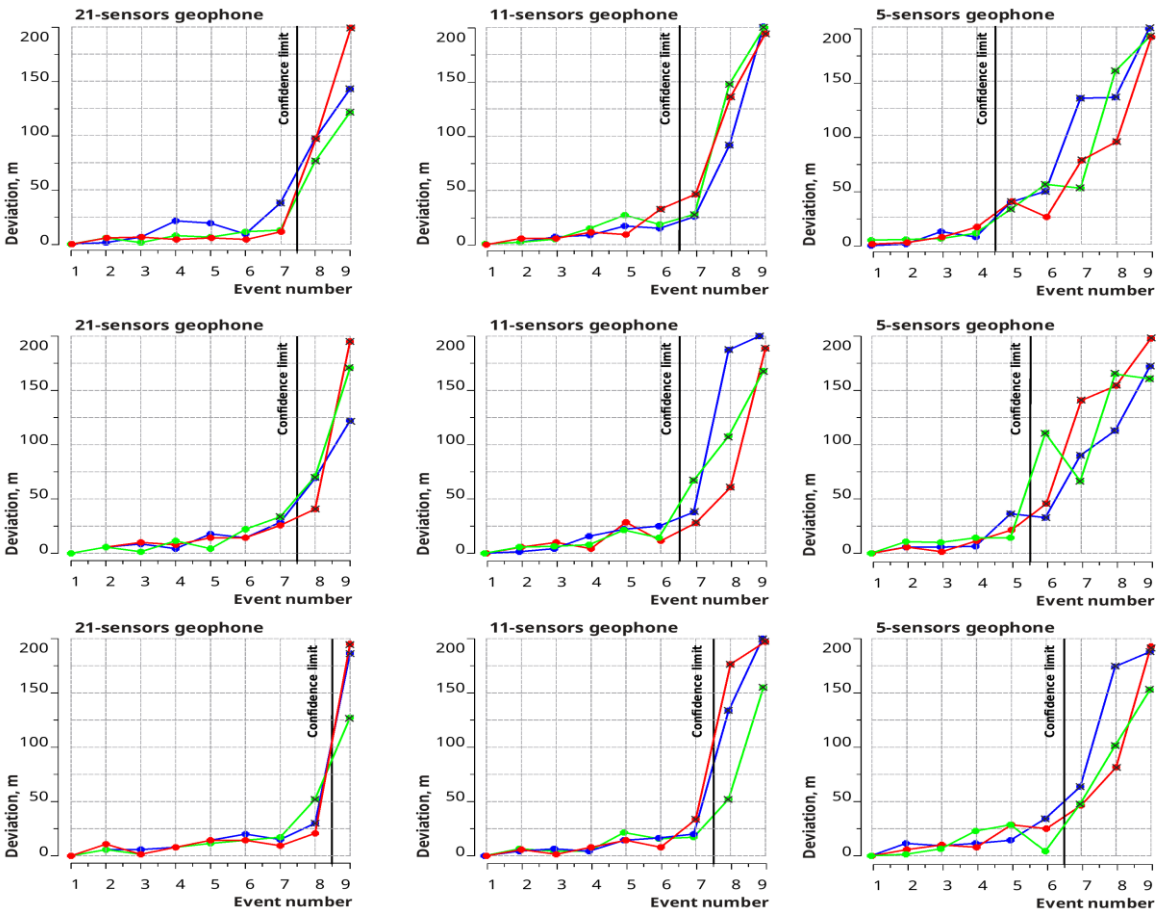

Event №	s / n
1	10
2	5
3	2.5
4	1.25
5	0.8
6	0.6
7	0.4
8	0.2
9	0.1

Fig. 6. Deviations of the estimated coordinates of the events from the specified

2. Surface survey Method

In a homogeneous (to exclude the factor of inaccuracy of knowledge of the model) section with velocities Vp=3500 m/s and Vs=1600 m/s at a depth of 1200 m, events were simulated on a straight line starting at the treatment well under study with a decreasing signal-to-noise ratio from 5 to 0.02 (Table 2). The receiving system consisted of three lines under 120^0 centered at the mouth of the well (Fig. 7, 8).

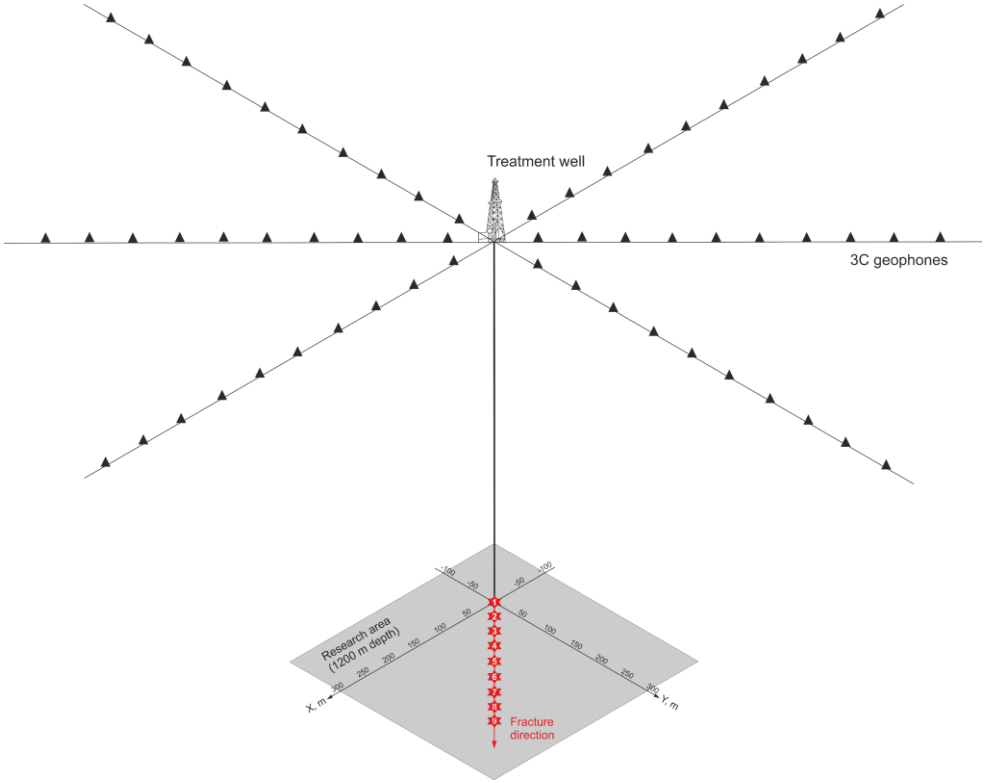

Fig. 7. Surface acquisition geometry

Model wavefields for one line (following component)

Pressure waves

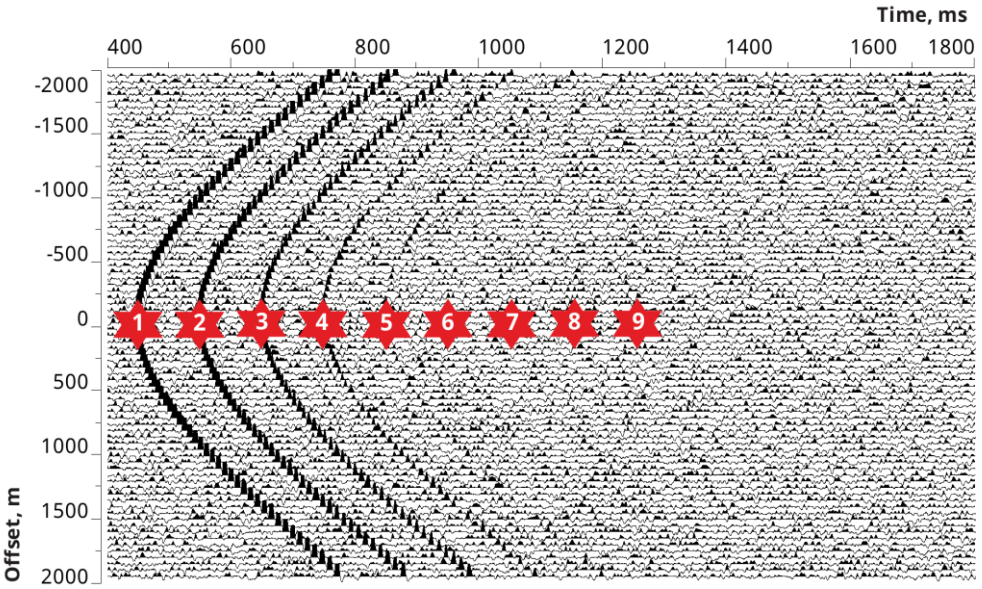

Shear waves

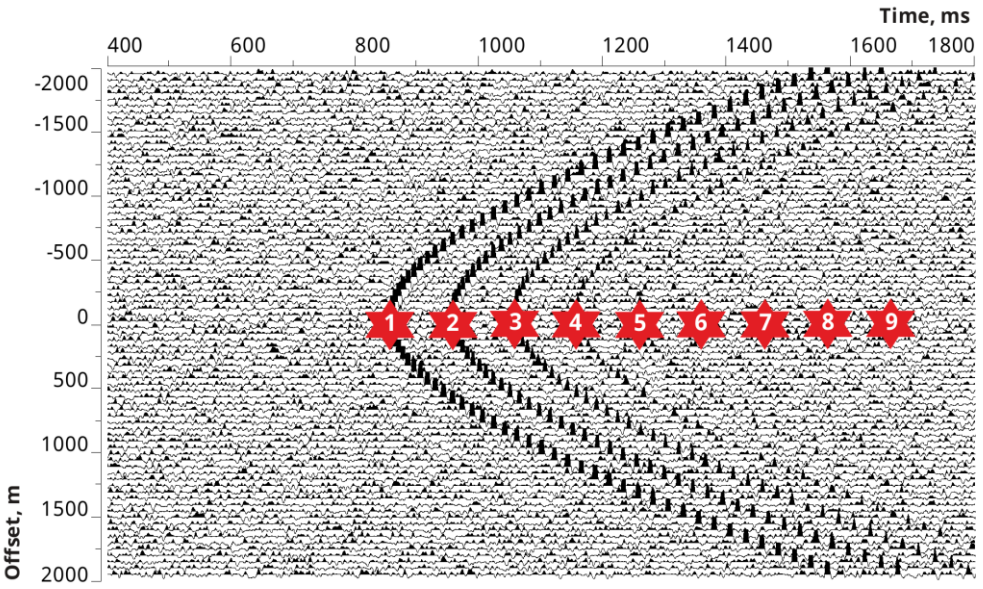

Fig. 8. Model wavefields (following component)

Table 2. Events with different signal to noise ratios

Event №	1	2	3	4	5	6	7	8	9
s / n	5	2.5	1.25	0.63	0.31	0.16	0.08	0.04	0.02

Fields of probability

The probability fields for the first event concentrate well near the point of formation, but are slightly stretched vertically. Localization is improved for pressure and shear waves processed together (Fig. 9).

When pressure and shear waves are used together, an error of up to 25 m is achieved for 240 sensors at s/n up to 0.04, for 120 sensors at s/p 0.08 and for 60 sensors at s/p 0.16 (Fig. 10-11).

Fields of probability

Pressure waves

Shear waves

Both pressure and shear waves

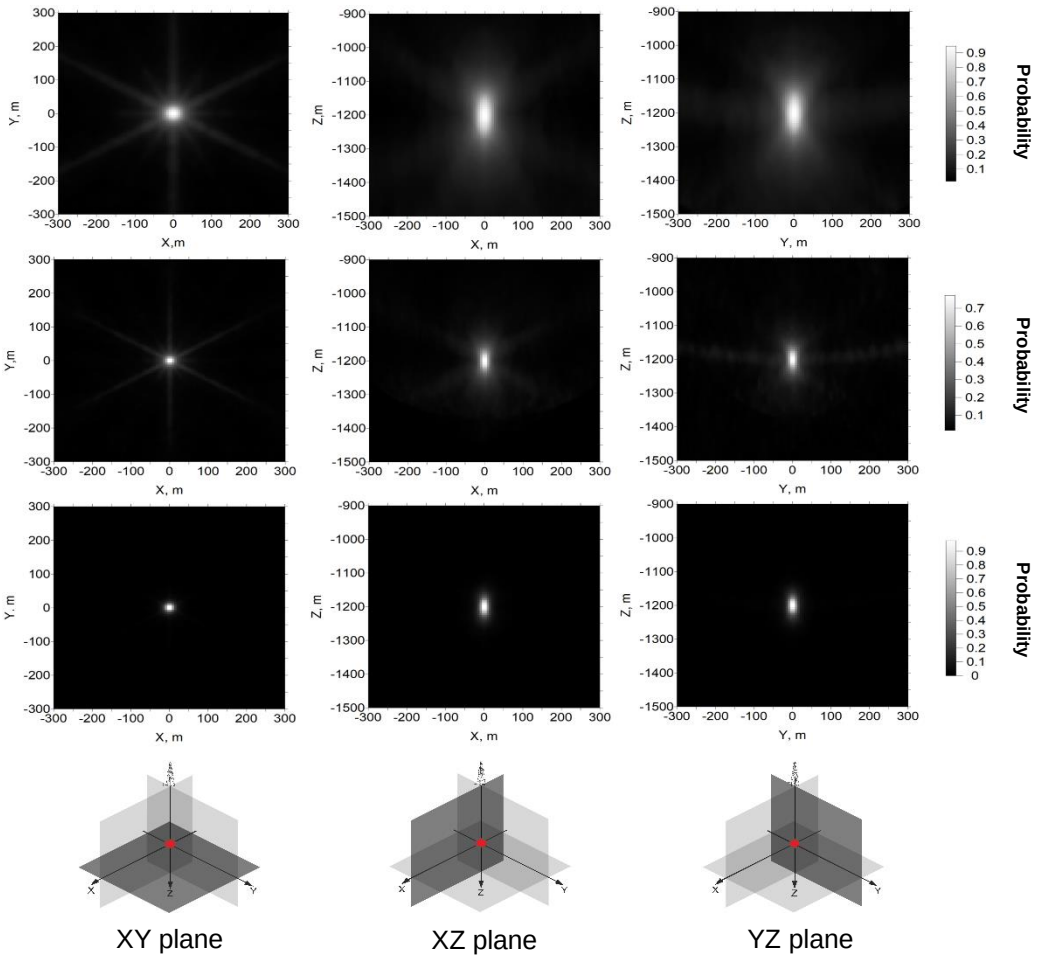

Fig. 9. Probability fields for the first event (240-sensor surface array, 120^0 aperture)

Localized microseismic events

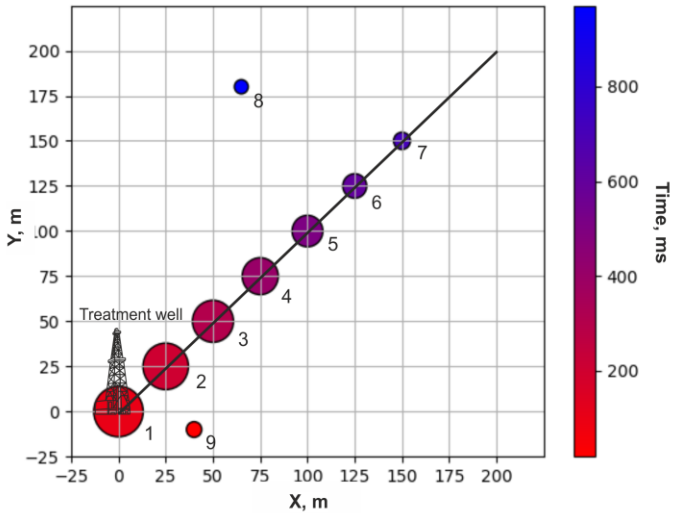

Pressure waves

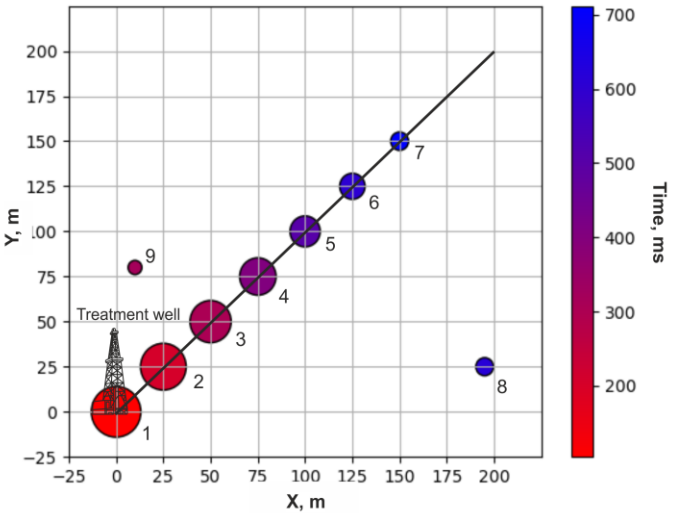

Shear waves

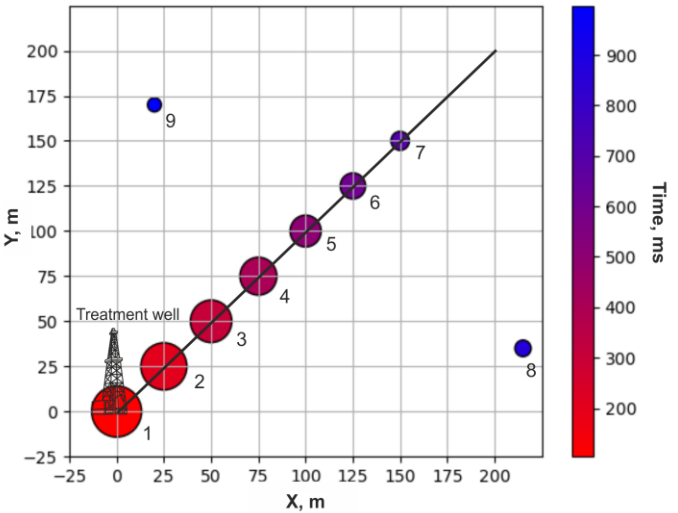

Both pressure and shear waves

Event №	1	2	3	4	5	6	7	8	9
s / n	5	2.5	1.25	0.63	0.31	0.16	0.08	0.04	0.02

Fig. 10. Expected localization points for the events (240-sensor surface array, 120^0 aperture)

Deviations of the estimated centers of microseismic events from the specified

Pressure waves

Shear waves

Both pressure and shear waves

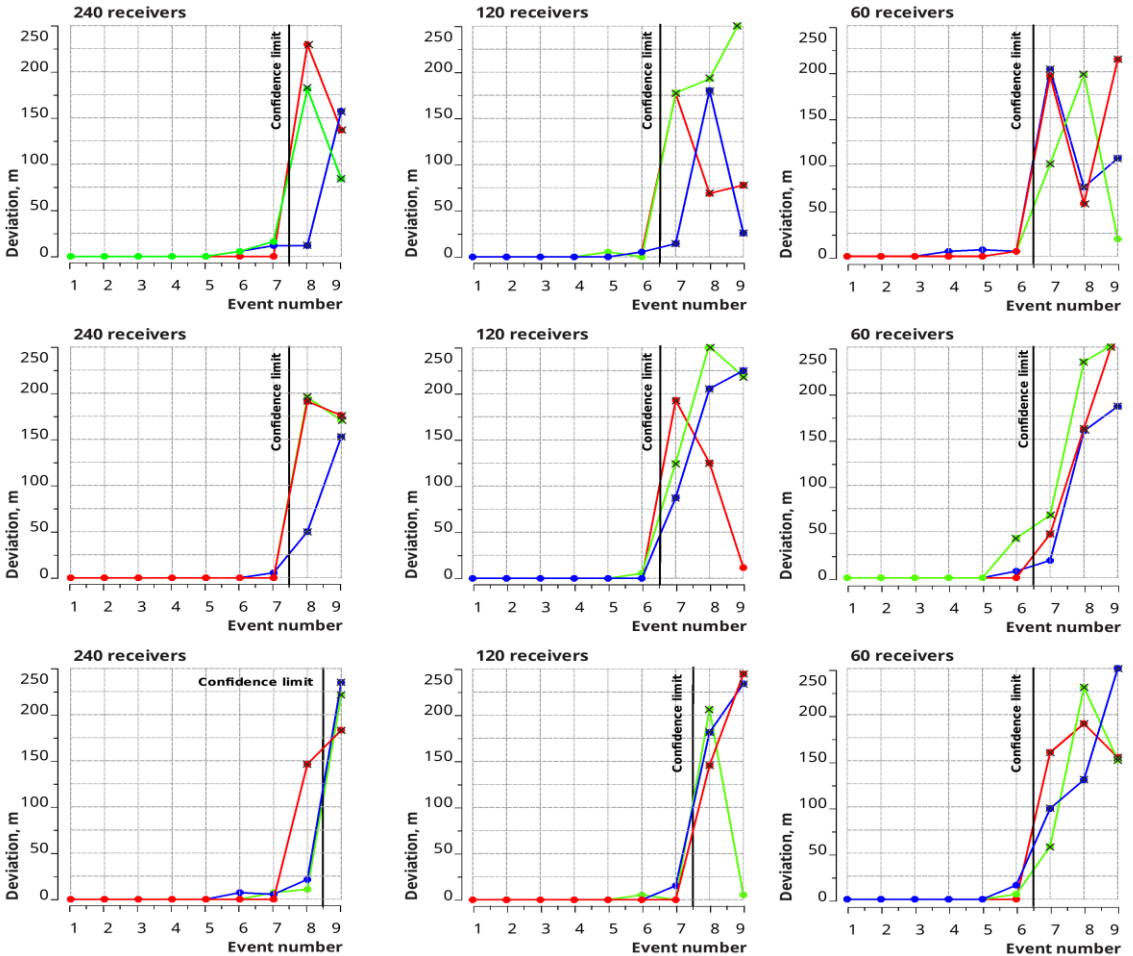

Event №	s / n
1	5
2	2.5
3	1.25
4	0.63
5	0.31
6	0.16
7	0.08
8	0.04
9	0.02

Fig. 11. Deviations of the estimated coordinates of the events from the specified

Conclusions

1. Technology of localization hydraulic fracturing events by seismic monitoring with Intellectual Robot ADEE provides high accuracy of automatic detecting and localization the events with high resistance to noises. Real time control of fracturing events becomes available.

2. Linear (borehole) antenna provides higher accuracy in spacing and smaller in lateral direction.

3. Joint usage of pressure and shear waves increases accuracy and noise resistance. Shear waves provides better localization in probability space due to higher curvature.

4. Noise resistance increases almost linearly with larger number of sensors.

Recomendations

The developed technique and technology for microseismic events localization using the intelligent robot ADEE can be used:

1. For real-time fracture control with high accuracy and noise immunity.

2. When designing Fracture Control during Hydraulic Fracturing (FCHF), to select parameters of the field procedure and to assess the reliability of the results of processing and interpretation of CTG data.

http://geovers.com